Experimental Study of Breakdown Time in a Pulsed 2.45-GHz ECR Hydrogen Plasma Reactor

O. Daniel Cortázar, Ana Megía-Macías, and Alvaro Vizcaíno-de-Julián

***Abstract*—An electron cyclotron resonance (ECR) plasma reactor developed at the European Spallation Source Bilbao has been operated in pulsed mode at 50 Hz to study the breakdown-process dynamics by time-resolved diagnostics. Injected power, reflected power, electrical-biased probe saturation current, and light emission were measured simultaneously for three different magnetic fields: under ECR, ECR, and asymmetric over ECR profiles. Gas pressure, power, and duty cycle have been used in a parametric study obtaining information about microwave (MW) coupling and plasma formation stages during the breakdown process. The study is relevant for designers that need to extract short beam pulses from a 2.45 ECR ion source for any application because the total breakdown time measured is defined as corresponding to reach the steady-state plasma parameters. A simple model of residual electron density evolution between pulses is proposed to describe the MW coupling as a function of incoming power and duty cycles.**

***Index Terms*—Electron cyclotron resonance (ECR) plasma source, plasma breakdown, pulsed ECR ion source.**

I. Introduction

PLASMA dynamics during breakdown and decay in pulsed plasma sources are of special interest for pulse-mode electron cyclotron resonance (ECR) ion source (ECRIS) design and other many application fields such as particle accelerator science, nuclear fusion reactors, and plasma processing industry [1]–[5]. An extensive research on this subject was conducted by different researchers with electrical probes, spectroscopy, and radiation diagnostics under a wide range of parameters for different plasmas [6]–[12]. In this paper, we present a study of the breakdown on ECR hydrogen plasma by means of four time-resolved simultaneous diagnostics: electrical-biased probe saturation current, emitted light, incoming power, and reflected power measurements oriented to obtain typical breakdown times. Three different magnetic field profiles to embed the plasma have been used: symmetric under ECR, symmetric ECR, and asymmetric over ECR. The main goal of this paper is to improve the knowledge about characteristic plasma formation times during a breakdown process that can help ECRIS designers reach better performances. We have some special interest in the understanding of plasma formation processes to obtain plasma optimization criteria on two mainstream research lines: high-current monocharged ion beams and multicharged ion production.

Manuscript received May 4, 2012; revised July 19, 2012; accepted September 26, 2012. Date of publication October 22, 2012; date of current version December 7, 2012. This work was supported by the European Spallation Source Bilbao Consortium.

O. D. Cortázar is with University of Castilla-La Mancha, 13170 Ciudad Real, Spain (e-mail: dcortazar@essbilbao.org).

A. Megía-Macías and A. Vizcaíno-de-Julián are with European Spallation Source Bilbao Consortium, Edificio Cosimet, 48940 Leioa, Spain.

Color versions of one or more of the figures in this paper are available online at http://ieeexplore.ieee.org.

Digital Object Identifier 10.1109/TPS.2012.2222933

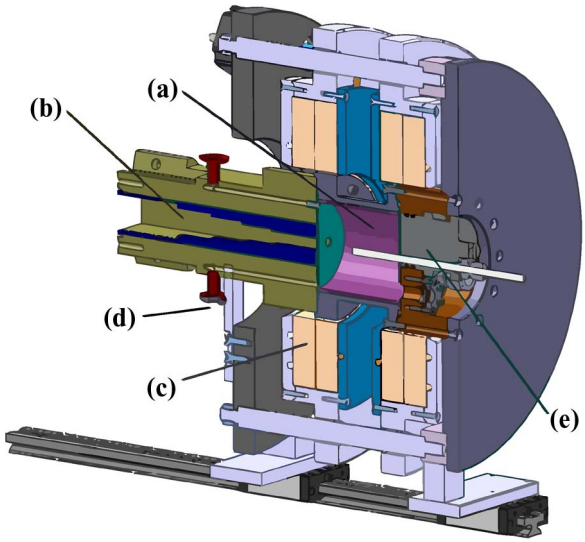

Fig. 1. View of plasma chamber and main subsystems. (a) Plasma chamber. (b) MW impedance adaptor. (c) Coil pancakes. (d) Pressure gauge inlet. (e) Diagnostic port.

II. Experimental Apparatus

A. Plasma Reactor

Measurements are made in a plasma reactor driven by a 3-kW adjustable power magnetron of 2.45 GHz that can be operated from a continuous wave to 20 kHz in pulsed mode. Fig. 1 shows a view of the reactor, including the main subsystems. The plasma chamber is cylindrical with a length of 93 mm and a diameter of 90 mm and is made of oxygen-free high-thermal-conductivity copper with an external water cooling bath for heat removal [see Fig. 1(a)]. A microwave (MW) is injected through one chamber side, whereas the opposite is used as vacuum pumping and diagnostic ports. From the MW injection side, a brass piece made with internal steps is used as a coupler for adapting impedances of the plasma chamber and WR 330 MW waveguides [see Fig. 1(b)]. A two-stub tuner is used for fine plasma impedance matching, and a directional coupler gives readings of incoming power and reflected power from the magnetron and the plasma, respectively. A 10-mm-thickness quartz window separates the vacuum enclosure from the MW driver system. A set of four coaxial coils [see Fig. 1(c)] arranged in two pancakes with independently variable circulating currents

of about 10 A can produce different magnetic field profiles by means of a positioning mechanism. Hydrogen is injected into the plasma chamber through a needle valve; its flow is measured by a digital flow meter, and its gas pressure is measured by a gauge connected to a body chamber [see Fig. 1(d)]. Both sides of the plasma chamber are covered by 2-mm-thickness boron nitride disks properly machined to fit the MW port, the gas inlet, and the diagnostic portholes. On the chamber diagnostic side, a lid is mounted, including a pumping port, a fused silica observation window, and a vacuum feedthrough for probes [see Fig. 1(e)]. Such lid is placed where the plasma electrode and the extraction system would be placed in the case when this reactor is used as an ECRIS. On the other hand, diagnostic port design permits taking measures by an electrical probe in the axis of the plasma chamber while hydrogen is pumped through the same centered hole. This issue was demonstrated to be important in our experiment for obtaining a symmetrical plasma density distribution with respect to the axis and has to be taken in consideration, particularly for low gas operating pressures. Clearly, our plasma reactor is an ECRIS reproduction without extraction electrodes [13]. The idea is to have a close reproduction of ISHP ion source under development at European Spallation Source Bilbao and to use it as a test bench for plasma research and optimization.

B. Magnetic Field Profiles

During reactor commissioning, start-up, and tuning stages, different magnetic field distributions were measured and tested. Some of them produced a strong plasma tendency to be allocated at the rear part of the plasma chamber (the MW injection side and the MW coupler piece).

Taking into account that the plasma quality close to the extraction zone is an important factor to reach good ECRIS performances, we consider such tendency as an undesired behavior. It evidently produces, in the best cases, low-density plasmas at the extraction zone. Careful attention was paid to establish the set of parameters where the plasma shows acceptable behaviors. This paper shows the results of the breakdown study for three different z-axis magnetic field profiles with a good behavior, taking as symmetry reference the center of plasma chamber ($z = 46$ mm).

Fig. 2 shows three B_z magnetic field profiles measured experimentally by a vector magnetic probe with a typical error of ± 1 mT. The plasma chamber limits are indicated by dotted vertical lines where the left border shows the MW injection side and the right border shows the diagnostic side. The ECR magnetic field level of 87.5 mT is marked by a dashed flat black line. Fig. 3 shows a 2-D calculations for each case of study, where the chamber is represented by a full black line and the ECR surface is the border between volumes of (violet) $B >$ ECR and (blue) $B <$ ECR. Note that the case (a) corresponds to a symmetric flat B_z magnetic field profile with values that are always under the ECR, case (b) corresponds to a symmetric B_z field with a value that is coincident to ECR, and case (c) is an asymmetrical profile with B_z that takes higher values that reach 120 mT. Such three magnetic field distributions were validated and were the experimental conditions that have been used during measurements, as typical operation modes, to check the influence of magnetic fields in plasma breakdown dynamics.

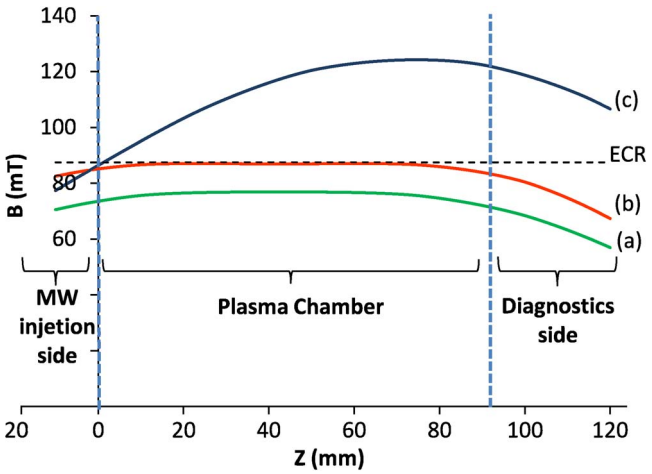

Fig. 2. Z-axis magnetic profiles used during experiments. (a) Symmetric $B_z <$ ECR magnetic profile. (b) Symmetric $B_z \simeq$ ECR profile. (c) Asymmetric $B_z >$ ECR magnetic profile.

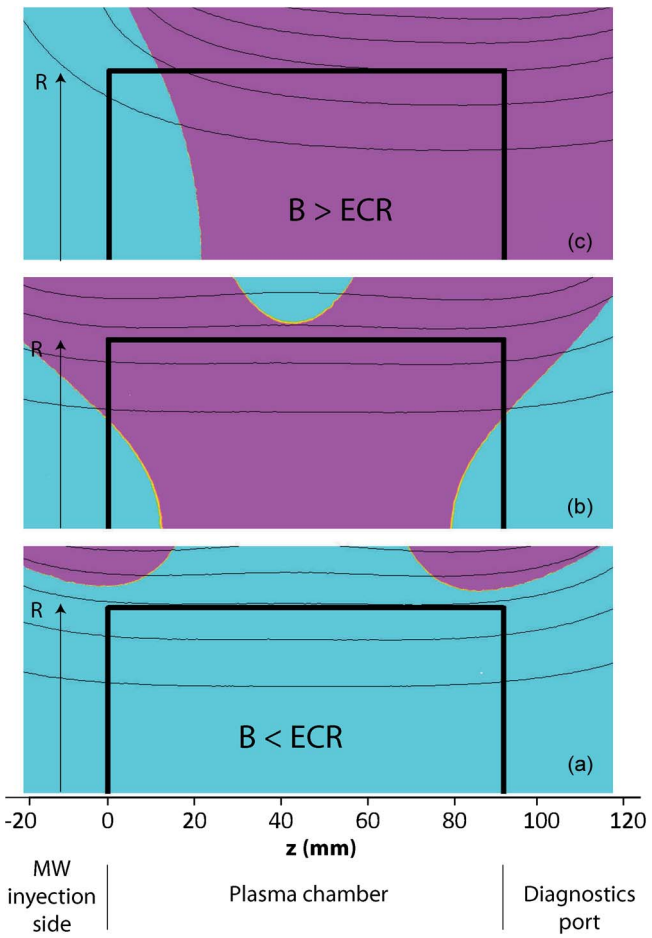

Fig. 3. Two-dimensional representation of magnetic profiles used during experiments showing the volumes for (violet) $B >$ ECR and (blue) $B <$ ECR, where the border between both volumes is the $B \simeq$ ECR surface for each case: (a) Symmetric $B_z <$ ECR magnetic profile; (b) Symmetric $B_z \simeq$ ECR profile; (c) Asymmetric $B_z >$ ECR magnetic profile. Symmetric half plasma chamber profile is represented by a full black line.

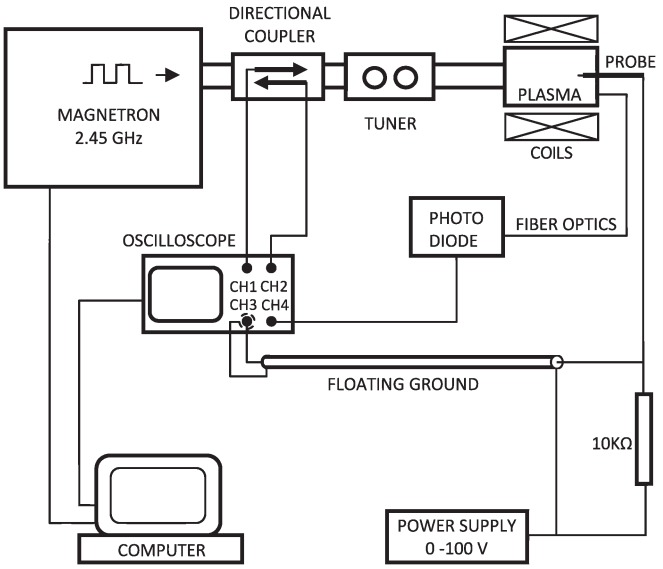

Fig. 4. Experimental setup for breakdown time measurement.

III. Breakdown Time Measurement

A. Experimental Arrangement

Four diagnostics have been conducted simultaneously for measuring characteristic breakdown times during pulsed operation at 50 Hz. Fig. 4 shows the experimental setup. Plasma injected power and reflected power are obtained by a bidirectional coupler. An electrical probe made of tungsten wire that is 6 mm long and has a 0.5-mm diameter is mounted inside a 1.5-mm-diameter aluminum tube placed in the center of the chamber ($r = 0$ and $z = 46$ mm). Such probe is polarized by a dc power supply at 100 V. By measuring the voltage across a resistor of 10 kΩ connected to the probe, the saturation electron current is obtained above the plasma space potential with a temporal resolution of 100 ns. A floating ground oscilloscope has been used because the probe ground floats at polarization voltage.

A fiber optics bundle with a diameter of 6.25 mm placed on the observation window is connected to a high-speed photodetector with a rise time of 14 ns, giving a signal proportional to the plasma light intensity emission. The range of observed wavelengths is 350–600 nm centered at 540 nm by using an optical collimator. Electron–ion recombination and neutral-gas-excitation spectral line contributions to light emission are both proportional to the product between electron and ion densities and inversely proportional to the square root of electron temperature [14]. We consider this light emission intensity signal as an interesting indicator of the ionization-process evolution. On the other hand, such signal has been very useful to detect anomalous behaviors related to plasma misplaced formation in the coupler piece or alternating breakdowns between the chamber and the injection side near the quartz window.

B. Measurement Procedure

A typical oscilloscope record of 64 averaged signals is shown in Fig. 5, where (a) is the injected power P_i, (b) is the reflected power P_r, (c) is the light intensity signal, and (d) is the current signal from the probe. These signals have been obtained under

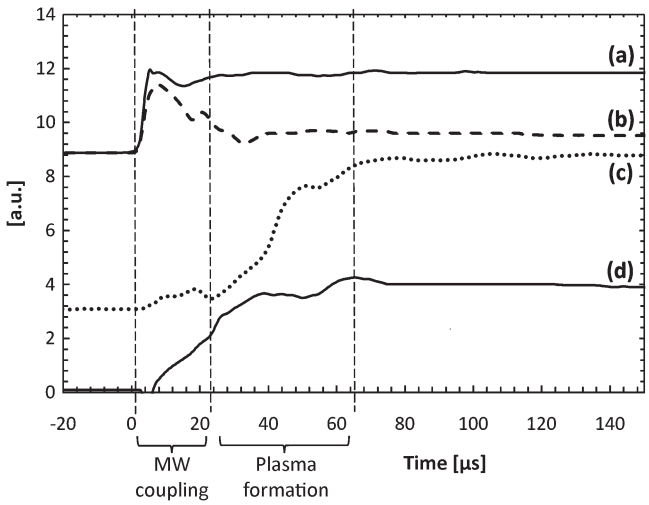

Fig. 5. Typical oscilloscope signal for measuring breakdown times. (a) Incoming power. (b) Reflected power. (c) Plasma emitted light. (d) Probe current.

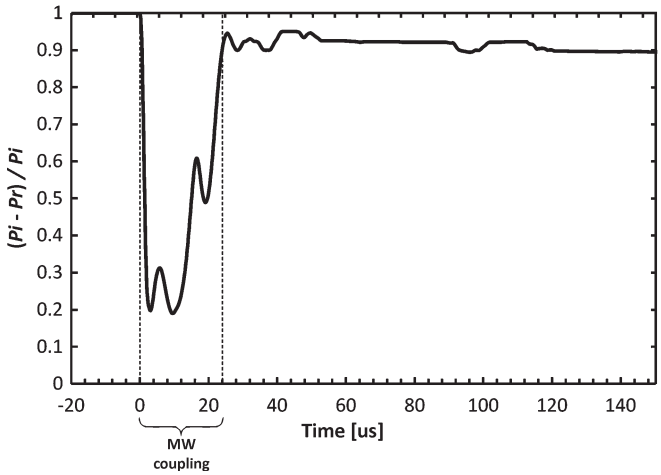

Fig. 6. Typical relative absorbed power $(P_i - P_r)/P_i$ calculated from direct measurements showing the MW-coupling time definition as proposed.

the following experimental conditions: frequency of 50 Hz, incoming MW power of 600 W, reflected MW power of 150 W, duty cycle of 70%, hydrogen pressure of 6.2×10^{-3} mbar, and the asymmetric magnetic profile shown in Fig. 2(c). The incoming power rise time of about 3 μs permits to make clear measurements of plasma breakdown evolution with respect to excitation. Fig. 5 shows a significant slope change on light and current signals simultaneously with a reflected power drop associated to MW coupling. It is reasonable to understand such instant as a characteristic time for a MW coupling process when an efficient power absorption is taking place. Fig. 6 shows the time evolution of the ratio between absorbed power $(P_i - P_r)$ and the incoming power P_i as calculated from direct measurements shown in Fig. 5. It is very significant how this relative absorbed power rises very fast when MW coupling is taking place. This process has been deeply associated to the drop of the electric field strength inside of the plasma chamber [9]–[11]. A deeper look in Figs. 5 and 6 suggests that plasma processes during breakdown may be understood as comprised by two stages.

TABLE I
PARAMETERS USED DURING THE EXPERIMENTS

Parameter	Values
Magnetic Field Profile	(a), (b) and (c) of Fig. 2
Hydrogen Pressure	3.8 and 6.2 x 10^{-3} mb
Peak MW Power (W)	300 to 1500 in steps of 300
Duty Cycle (%)	10 to 90 in steps of 10
Magnetron pulse frequency	Constant at 50 Hz
Probe Polarization (V)	Constant at 100 V

MW Coupling: The first stage is during which the MW power matching is in progress. This is an early breakdown stage characterized by a low ionization rate and a fast coupling dynamics between MWs and the weak plasma inside the chamber. This process can be deeply associated to the drop of the electric field strength inside of the plasma chamber according to the behavior of the absorbed power [9]–[11]. We define here the characteristic time of this stage as the time when relative absorbed power $(P_i - P_r)/P_i$ rapidly increases.

Plasma Formation: The second stage is during which light emission increment is associated to an improving ionization rate and where the saturation probe current is rapidly reached. During this period, the MW coupling is well established, and the absorbed energy density is good enough to produce plasma evolution to final steady-state parameters. Saturation in both light emission and probe current signals is recorded at practically the same time during the plasma formation stage. At first glance, we do not detect any remarkable influence of temperature variations during plasma formation time. We define here the characteristic time of this stage as the time where saturation in light emission and probe current is reached.

Fig. 5 shows the structure that is just proposed. According to such interpretation, we understand the breakdown time as the sum of these two partial times. Note that the only measurement of injected power and reflected power is not enough to observe the second stage of the plasma evolution doing what is necessary to implement other complementary diagnostics. Therefore, our definition involves all the time-resolved diagnostics conducted in this paper.

IV. RESULTS

Measurements are conducted to obtain MW coupling, plasma formation, and total breakdown times. The range of parameter variation during experiments is shown in Table I. Three main cases are studied for the three magnetic field profiles detailed in Fig. 2, where each one is studied for two hydrogen operation pressures by scanning injected power and duty cycles between 300–1500 W and 10%–90%, respectively. Magnetron pulse frequency of 50 Hz and the probe polarization voltage of 100 V are both constant.

A. Breakdown Time Measurements With Magnetic Field Profiles in Figs. 2(a) and 3(a): Symmetrical $B_z <$ ECR

Fig. 7 shows measurements corresponding to hydrogen pressures of 3.8×10^{-3} mbar, where the times are represented as surfaces obtained by linear interpolation between measured points. The times are plotted as a function of MW incoming power and duty cycles, where Fig. 7(a) shows the MW coupling time, Fig. 7(b) shows the plasma formation time, and Fig. 7(c) shows the total breakdown time as the sum of previous values. In general terms, the plasma behavior for this relatively low $B_z <$ ECR profile is unstable, showing a narrow range of power values where measures could be conducted always with a poor coupling, low emitted light intensity, and a remarkable jitter. Fig. 7(a) shows MW coupling times where a narrow power range between 1200 and 1500 W is the only one possible and where some measurements could be done. For this cases, the system presents a poor MW coupling with high reflected MW power values. The rest of the power values and duty cycles tested present a behavior characterized by high jitter or even plasma allocation outside of the plasma chamber. Such high-jitter behavior practically disregards these data for any application related to reasonable reproducibility. Fig. 7(a) does not show data in such experimental conditions, and the corresponding parameter's area looks empty. Fig. 7(b) shows plasma formation times practically with the same behavior and always with values between 40 and 80 μs. Fig. 7(c) shows the total breakdown time as the sum of previous values reaching maximum values of 180 μs at 40% of duty cycles.

Fig. 8 shows the measurements corresponding to the hydrogen higher pressure of 6.2×10^{-3} mbar, where times are represented, as in the previous figure, and plotted as function of MW incoming power and duty cycles. Fig. 8(a) is the MW coupling time, Fig. 8(b) is the plasma formation time, and Fig. 8(c) is the total time as the sum of the previous values. This case shows a more reproducible behavior where MW coupling time starts as low as 10 μs at high power values, and it gradually increases, reaching 50 μs for low power values. Particularly interesting is the corner of low power about 300 W and high duty cycles of 80%–90%, where an unstable area with high jitter is founded and data are not possible to record. Such area is represented in Fig. 8 as empty. It is important to remark that these horizontal surfaces are not representing saturation regions. Such areas are unstable regions where the breakdown process is nonpredictable and representing the cutoff values from where the influence of the high jitter does not permit to take useful data.

Fig. 8(a) shows that MW coupling times remain practically constant and take values ranging from 20 to 50 μs. An exception is recorded at the corner of low power and high duty cycles where unstable area aforementioned is founded. Plasma formation time is shown in Fig. 8(b), where it can be seen that smaller values around 70 μs are obtained for high power and low duty cycles, whereas the rest of the surface is characterized by a saddle-like shape that reaches higher values of 150 μs at low power values and high duty cycles just before the flat top unstable high-jitter area. The total breakdown time is shown in Fig. 8(c) as the sum of previous surfaces. The plasma formation time surface is mainly reflected on the breakdown time surface, keeping it the same with the shape in Fig. 8(b) with an unstable area at the top. However, the faster breakdown times keep values of 70 μs in the corner of high power and low duty cycles where good coupling conditions are evident.

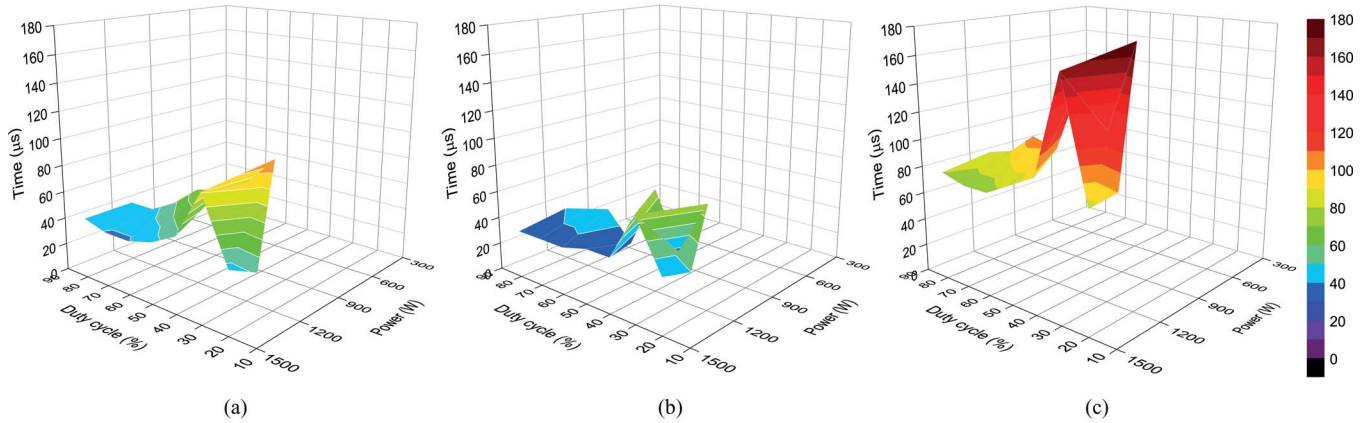

Fig. 7. Breakdown times for $B_z <$ ECR magnetic field distribution corresponding to Figs. 2(a) and 3(a) for a hydrogen pressure of 3.8×10^{-3} mbar. (a) MW coupling time. (b) Plasma formation time. (c) Total breakdown time as the sum of the previous values.

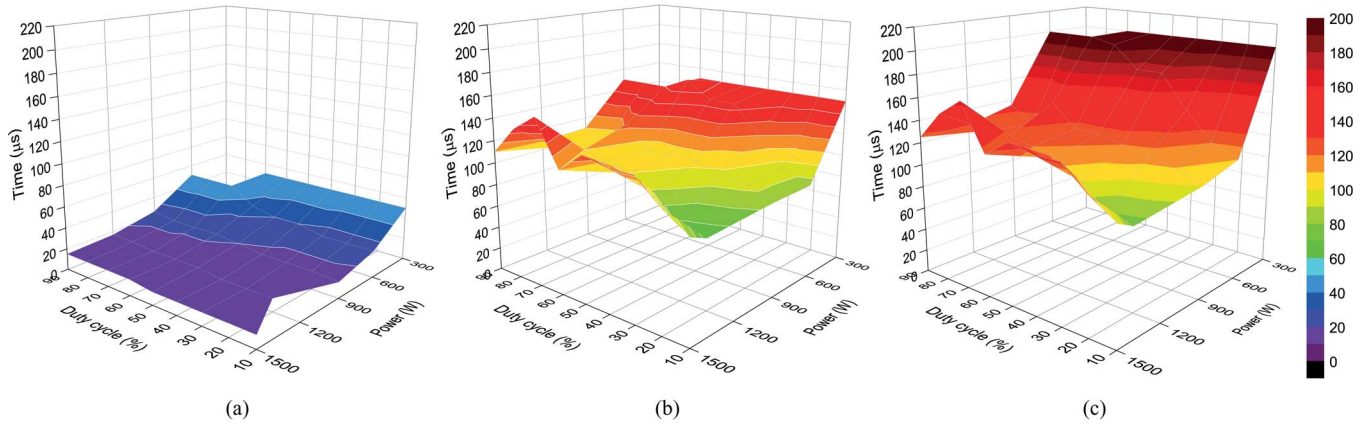

Fig. 8. Breakdown times for a flat $B_z <$ ECR magnetic field distribution corresponding to Figs. 2(a) and 3(a) for a hydrogen pressure of 6.2×10^{-3} mbar. (a) MW coupling time. (b) Plasma formation time. (c) Total breakdown time as the sum of the previous values.

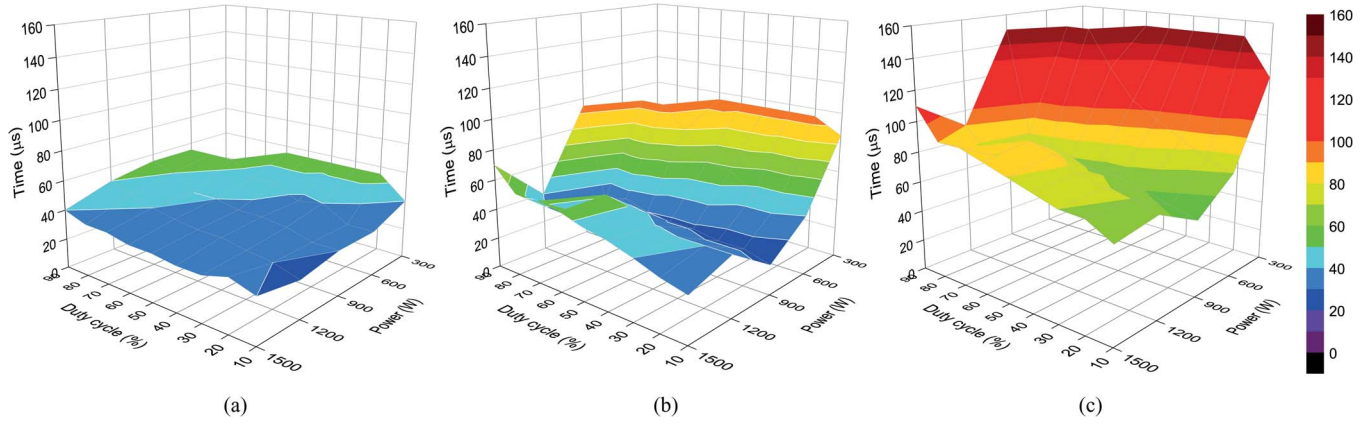

Fig. 9. Breakdown times for a flat $B_z \simeq$ ECR magnetic field distribution corresponding to Figs. 2(b) and 3(b) for a hydrogen pressure of 3.8×10^{-3} mbar. (a) MW coupling time. (b) Plasma formation time. (c) Total breakdown time as the sum of previous values.

B. Breakdown Time Measurements With the Magnetic Field Profiles in Figs. 2(b) and 3(b): Symmetrical $B_z \simeq$ ECR

Plasma behavior at $B_z \simeq$ ECR is stable, showing a relative wide range of power values and duty cycles, where measures can be conducted always with good coupling and high emitted light intensity. Fig. 9 shows the measurements corresponding to hydrogen pressures of 3.8×10^{-3} mbar. Breakdown times are plotted as a function of MW incoming power and duty cycles: Fig. 9(a) is the MW coupling time, Fig. 9(b) is the plasma formation time, and Fig. 9(c) is the total time as the sum of previous values. For this experimental condition, the dependence of MW coupling time shown in Fig. 9(a) remains practically constant between values from 30 to 50 μs, showing a slightly growing tendency from low duty cycles and high power to high duty cycles and low power. On the other hand, plasma formation times in Fig. 9(b) show a different

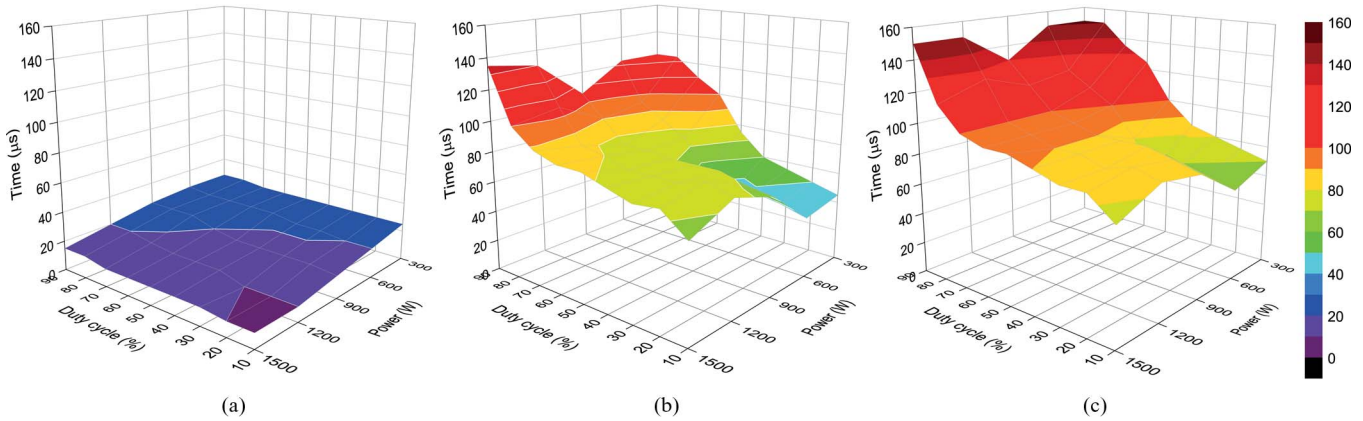

Fig. 10. Breakdown times for a flat $B_z \simeq$ ECR magnetic field distribution corresponding to Figs. 2(b) and 3(b) for a hydrogen pressure of 6.2×10^{-3} mbar. (a) MW coupling time. (b) Plasma formation time. (c) Total breakdown time as the sum of previous values.

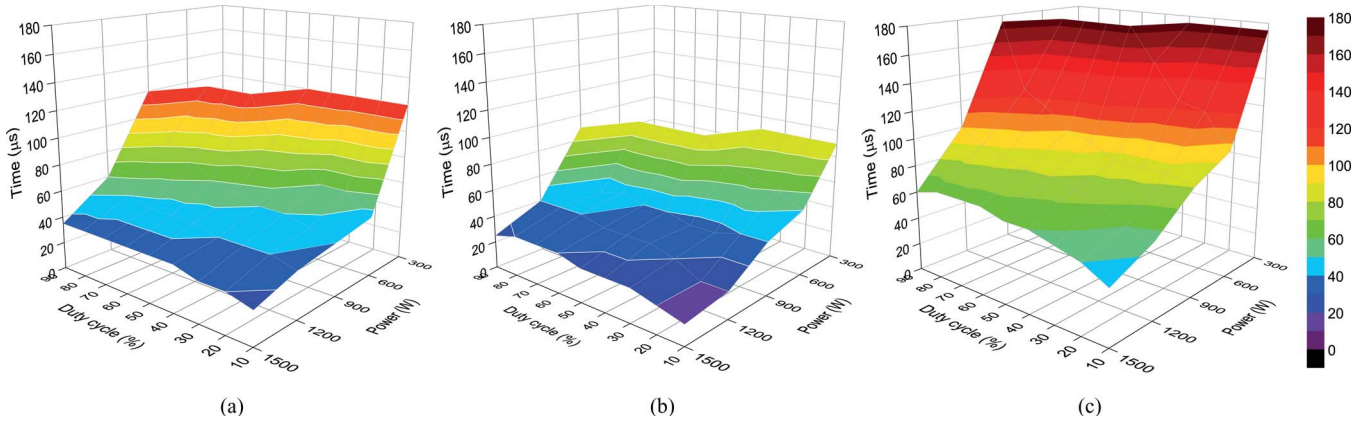

Fig. 11. Breakdown times for a flat $B_z >$ ECR magnetic field distribution corresponding to Figs. 2(c) and 3(c) for a hydrogen pressure of 3.8×10^{-3}. (a) MW coupling time. (b) Plasma formation time. (c) Total breakdown time as the sum of the previous values.

behavior characterized by a significant drop along the line of middle power values about typically 900 W. Such times are relative high, starting at values of 40 μs and reaching 95 μs at the corner of low power values and high duty cycles. Total breakdown times are shown in Fig. 9(c), where the influence of plasma formation times in the surface shape is clear. Breakdown times that reach 150 μs for lower values of power and high duty cycles just before entering in the unreliable area of high-jitter behavior are in contrast with the faster values of 50 μs at the opposite corner of high power values and low duty cycles.

Fig. 10 shows the cases corresponding to hydrogen pressures of 6.2×10^{-3} mbar embedded in $B_z \simeq$ ECR. The same scheme of the previous figure is followed; the plots are function of MW incoming power and duty cycles: (a) is the MW coupling time, (b) is the plasma formation time, and (c) is the total time as the sum of previous values. Note that the MW coupling times in Fig. 10(a) are faster than the previous lower pressure case, remaining practically constant at values of 20–30 μs and showing a better coupling behavior independent of duty cycle and power variations. A different situation is shown in Fig. 10(b), where the range of power values and duty cycles studied shows a strong tendency to increase the plasma formation times to values that reach 130 μs while the duty cycles are increased. It is remarkable how coupling and plasma formation times show an opposite behavior when hydrogen pressure is increased. While the first one reduces, showing faster coupling dynamics, the second one increases, showing the necessity of more time for plasma parameter evolution. Such two opposite dynamics are practically compensated in the calculation of total breakdown time, which Fig. 10(c) shows, in comparison with the previous lower pressure case. However, this surface starts at higher values, showing a soft growing tendency between 70 and 150 μs from low to high duty cycles, respectively. Another issue is the absence of the depression corresponding to the middle-value MW power at 900 W, which is present at lower pressure.

C. Breakdown Time Measurements With Magnetic Field Profiles in Figs. 2(c) and 3(c): Asymmetrical $B_z >$ ECR

In general, plasma behavior at $B_z >$ ECR is stable, showing a wide range of power values and duty cycles where measures can be conducted always with good coupling and high emitted light intensity. Fig. 11 shows the times corresponding to hydrogen pressure of 3.8×10^{-3} mbar. Such times are plotted as function of MW incoming power and duty cycles, where Fig. 11(a) is the MW coupling time, Fig. 11(b) is the plasma formation time, and Fig. 11(c) is the total time as the sum of

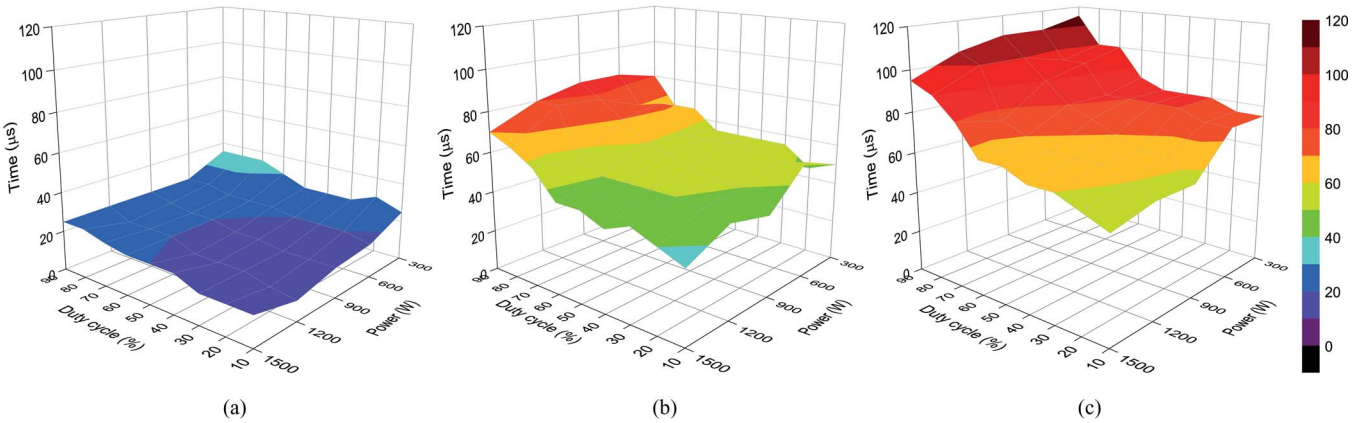

Fig. 12. Breakdown times for a flat $B_z >$ ECR magnetic field distribution corresponding to Figs. 2(c) and 3(c) for a hydrogen pressure of 6.2×10^{-3} mbar. (a) MW coupling time. (b) Plasma formation time. (c) Total breakdown time as the sum of previous.

previous values, as aforementioned. The change in the MW coupling time under this experimental conditions is remarkable, which shows a tendency to grow while power decreases, as shown in Fig. 11(a). For this case, it is evident that faster coupling times are strictly engaged to MWs with higher incoming power while the dependence with the duty cycle is relative smooth. Other interesting issue is the relative wide range of variation where lower values start at 20 μs, reaching 120 μs in the high duty cycle and the low power region. Fig. 11(b) shows clearly how plasma formation times are relative faster with respect to previous cases, where longer times are needed for reaching the final plasma steady state. For this case, the maximum value reached for plasma formation time is 90 μs, whereas the minimum is 10 μs at the corner of high MW power and low duty cycles. Such behavior is reflected in Fig. 11(c), where the total breakdown time is represented as the sum of the previous ones. It is clear that the main slope follows the MW power, reaching values of 180 μs for high duty cycles and low MW power values, whereas the opposite corner of low duty cycles and high power is characterized by low breakdown times of 50 μs. It is remarkable that, for all cases, the breakdown time always evolves toward an unstable area where jitter makes the phenomena completely unpredictable. From the point of view of reproducibility and applicability to the design of an ECRIS, the existence of such unstable areas represents a serious limitation. Fig. 12 shows the times corresponding to hydrogen pressures of 6.2×10^{-3} mbar embedded in $B_z >$ ECR. The same scheme of the previous figure is followed, where the plots are the function of MW incoming power and duty cycles. Note how Fig. 12(a) shows that MW coupling time comes back to a behavior of practically flat surface and lower values for the range of power values and duty cycles studied, as in previous cases of $B_z \simeq$ ECR. No remarkable slopes are recorded for this case, and values are in the range of 10–30 μs, showing a fast MW coupling. Fig. 12(b) shows a significant growing tendency of plasma formation time when the duty cycle is increased. Note how the maximum values are reached at 90% of the duty cycle, where a smooth curve with a maximum value of 85 μs at 900 W is recorded. This behavior is reflected in Fig. 12(c), where total breakdown time receives the influence of plasma formation time, reaching the maximum value of 110 μs and the minimum value of 40 μs. In general terms, comparison between both pressures at $B_z >$ ECR is interesting because the surfaces of total breakdown time show different behaviors. The lower pressure case presents a more aggressive changing behavior, depending to the MW power values, and the higher pressure case shows the lowest value at the corner of high power and low duty cycles. Other interesting issue is that, under this last pressure regime, no unstable high-jitter area is observed.

V. Simple Model of Breakdown Time

The pressure dependence of breakdown time can be understood by means of the model proposed in [6], where

$$t_{\text{breakdown}} = \tau_{\text{ion}} \ln(n_{e,\text{critical}}/n_{e0}) \tag{1}$$

where $t_{\text{breakdown}}$ is the breakdown time, $\tau_{\text{ion}} = [n_n \langle \sigma_{\text{ion}}\, v \rangle]^{-1}$ is the characteristic ionization time, σ_{ion} is the ionization cross section, v is the relative velocity (electron and neutral particles) with $\langle\rangle$ denoting the average over the velocity distribution, n_n is the neutral gas density, $n_{e,\text{critical}}$ is the critical value that the electron density have to reach for producing breakdown, and n_{e0} is the electron density in the plasma chamber at the beginning of the MW pulse. Assuming that, during breakdown, $\langle \sigma_{\text{ion}}\, v \rangle$ and n_n are independent of time, (1) predicts that the time required for plasma breakdown is inversely proportional to neutral particle density. It was checked successfully with different gas species, giving the order of magnitude rightly. The strong impact of the initial electron density n_{e0} at the instant that MW pulse starts is also predicted by (1). Considering that this initial value is the final value of the seed electron density evolution during plasma offtime that comes from the decay of the previous pulse, the dependence of breakdown time with incoming power and duty cycle may be studied.

We now consider a simple model just to explain our experimental results. Accepting that, after MW excitation pulse is off, an electron density remains embedded in the neutral gas during a time that is long enough to produce some influence in the breakdown of the following pulse, such density should evolve between pulses (plasma offtime), decreasing according to a rate of recombination with ions and a radial diffusion under the

influence of magnetic field applied inside the chamber. Under these assumptions, the electron density evolution should obey the following:

$$\frac{dn_e}{dt} = D_e \nabla^2 n_e - n_e n_i \langle \sigma_{\rm rec}\, v \rangle \tag{2}$$

where D_e is the ambipolar diffusion coefficient for ECR plasmas, n_e is the electron density, n_i is the ion density, $\sigma_{\rm rec}$ is the recombination cross section under the magnetic field influence, v is the relative velocity (electrons and ions), and $\langle\rangle$ denotes the average over the velocity distribution. Assuming that $\langle \sigma_{\rm rec}\, v \rangle$ remains practically constant, $n_e = n_i = n$ during the recombination process, and cylindrical symmetry is infinite, (2) takes the following shape in the cylindrical coordinates:

$$\frac{dn}{dt} = \frac{D_e}{r}\frac{\partial}{\partial r}\left(r\frac{\partial n}{\partial r}\right) - n^2 \langle \sigma_{\rm rec}\, v \rangle. \tag{3}$$

This equation was solved in [15] with the following dimensionless variables:

$$N = n/n_{\rm res}; \quad \tau = tD_e/\Lambda; \quad \Lambda = R/\lambda_1; \quad \rho = r/\Lambda$$

where, for our case, we use $n_{\rm res}$ as the residual value of n_e soaked in neutral gas immediately after the plasma is off in the z-axis ($r = 0$), R is the plasma chamber radius, and $\lambda_1 = 2.405$ for cylindrical symmetry obtaining:

$$\frac{dN}{d\tau} = \frac{1}{\rho}\frac{\partial}{\partial \rho}\left(\rho\frac{\partial N}{\partial \rho}\right) - \beta N^2 \tag{4}$$

with the following boundary conditions:

$$N(\lambda_1, \tau) = 0 \quad ; \quad N(\rho, 0) = J_0(\rho)$$

where the first condition is the zero density condition at the plasma chamber wall, and the second condition is the initial radial density distribution assumed as Bessel's function by solving (2) at $t = 0$. Note that (4) has only one parameter, i.e.,

$$\beta = \frac{\langle \sigma_{\rm rec}\, v \rangle n_{\rm res} \Lambda^2}{D_e} = \frac{\langle \sigma_{\rm rec}\, v \rangle n_{\rm res}^2}{n_{\rm res} D_e/\Lambda^2} \tag{5}$$

that can be understood as the ratio between the initial axial electron loss rate in the absence of diffusion, and the corresponding loss rate resulting from only diffusion. Thus, β is a measure of the degree to which the plasma is initially recombination controlled ($\beta \gg 1$) or diffusion controlled ($\beta \ll 1$). In our case, to calculate β, we need to estimate $\langle \sigma_{\rm rec}\, v \rangle$ and D_e. Assuming that, during plasma offtime between pulses, seed electrons are at 1 eV of temperature (order of magnitude estimation), we can use the approximation [16] for a neutral hydrogen plasma as follows:

$$\langle \sigma_{\rm rec}\, v \rangle = 0.7 \times 10^{-19} \left(\frac{13.6}{T_e(eV)}\right)^{1/2} \tag{6}$$

and the Bhom semi-empirical approximation [17] to estimate the diffusion coefficient for an ECR plasma as follows:

$$D_{\rm Bhom} = \frac{kT_e}{16eB}. \tag{7}$$

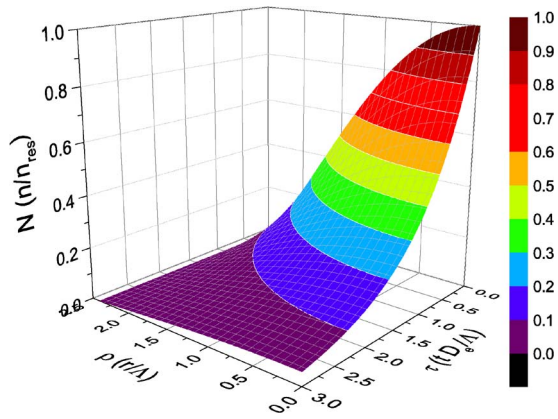

Fig. 13. Calculation of density temporal and spatial evolution.

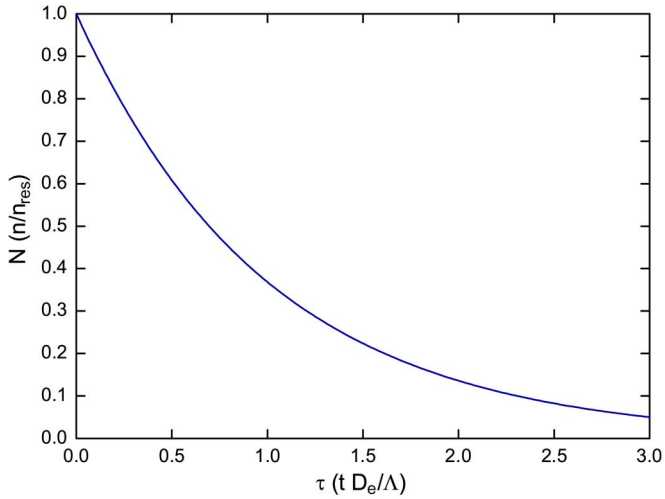

Fig. 14. Calculation of seed electron density temporal evolution at $r = 0$.

Considering the ECR magnetic field and taking an initial electron density deliberately high, such as the typical measured value of 10^{16} m^{-3} during the flat top pulse, to check the best of cases for collisions with ions and the worst of cases for the diffusive regime, we have

$$\beta = 3.8 \times 10^{-6} \ll 1. \tag{8}$$

It shows that, for our ECR plasma, the predominant initial condition is completely diffusive, even considering the best parameter set for collisions. This calculation confirms the behavior proposed in [17] on the basis of experimental data. The solution of (2) is shown in Fig. 13, where the diffusive behavior can be observed by looking how the radial density distribution of the Bessel's function profile decays progressively with time. Particularly interesting for our experimental data comparison is the level curve at $r = 0$ because this is the position that our electrical probe was placed during measurements. Fig. 14 shows this curve where time electron density evolution is shown. On the other hand, taking into account that characteristic ionization time in (1) is $\tau_{\rm ion} = [n_n \langle \sigma_{\rm ion}\, v \rangle]^{-1}$, if we assume approximation $\langle \sigma_{\rm ion}\, v \rangle \approx \sigma_{\rm ion} \langle v \rangle$, we can relate $\langle v \rangle$ with the incoming power by using the Fokker–Planck-based model proposed in [18]. This model proposes that electron dynamics of plasma cyclotron heating is driven by an energy

transfer mechanism between highly energetic electrons (that are directly accelerated by radio frequency) and a population of low-temperature electrons. The dynamical friction force that produces such energy transfer is calculated as proportional to $\langle v \rangle$, and the rate of transferred energy is proportional to $\langle v \rangle^2$. Under these assumptions and considering that neutral gas density n_n is proportional to neutral gas pressure, we can estimate the characteristic ionization time by

$$\tau_{\text{ion}} \approx \tau_{\text{ionmin}} \frac{p_{\max}}{p} \sqrt{\frac{P_{\max}}{P}} \tag{9}$$

where τ_{ionmin} is the minimum order of magnitude of the characteristic ionization time estimated from our data corresponding to maximum power and neutral gas pressure used in our experiments, $p_{\max}$ is the maximum neutral gas pressure, $P_{\max}$ is the maximum value of power, p is pressure, and P is power. Finally, (1) takes the following shape:

$$t_{\text{breakdown}} \approx \tau_{\text{ion}} \ln \left(\frac{n_{e,\text{critical}}}{n_{\text{res}}} \frac{1}{N} \right) \tag{10}$$

with τ_{ion} from (9) and N coming from calculations shown in Fig. 14 by converting dimensionless time to real time and using the offtime between pulses $\tau_{\text{off}} = (1 - DC/100)/f$, where DC is the duty cycle and f is the operation pulse frequency. By using $P_{\max} = 1500$ W, $p_{\max} = 6.2 \times 10^{-3}$mbar, and $f = 50$ Hz, we estimate by (10) the order of magnitude of breakdown time as a function of duty cycle and power under the following assumptions.

1) MW coupling is the more significant factor related to the breakdown time calculated by (1) because the process of ionization by collisions is mainly driven by the electric field enhancement produced during such stage.
2) Minimum characteristic ionization time is estimated from ECR MW coupling times shown in Fig. 9(a), where the order of magnitude is about 1 μs. This is coincident with the calculations of optimal breakdown conditions in am ECR 2.45-GHz plasma in [18].
3) The ratio $n_{e,\text{critical}}/n_{\text{res}} = 10^6$ is assumed to keep the assumption of $n_{e,\text{critical}}/n_{e0} = 10^7$ used in [6], considering the variation range of N.

Fig. 15 shows two surfaces calculated for our working pressures of 3.8×10^{-3}mbar and 6.2×10^{-3}mbar. By comparing theses surfaces with Figs. 9(a) and 10(a), respectively, it can be seen that MW coupling time data match the order of magnitude with calculations. Note that constant minimum breakdown times about 20 μs are obtained over all range of duty cycles at 1500 W for both pressures cases. High incoming power values may produce high residual electrons with the consequence of a high enough seed electron density at the beginning of pulses. This can guarantee fast coupling in a wide range of duty cycles. Under this circumstances, saturation of faster coupling times with respect to duty cycle may be produced, as shown in Figs. 9(a) and 15.

However, a completely different situation is observed in our case for magnetic fields over ECR. Observing data shown in Figs. 11(a) and 12(a), there are significant differences between calculations and experimental data. Particularly interesting is

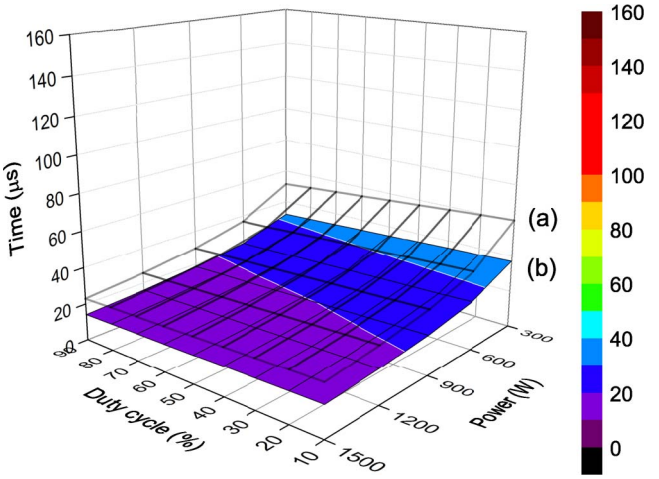

Fig. 15. Calculation of breakdown times for (a) 3.8×10^{-3}mbar and (b) 6.2×10^{-3}mbar.

the case of lower pressure at 3.8×10^{-3} mbar shown in Fig. 11(a), where the extended range of measured values and the increment of breakdown times are not described for our simple model.

VI. Summary and Conclusion

An experimental study of breakdown time in a 2.45-GHz hydrogen plasma reactor has been presented for three different magnetic field profiles, i.e., $B_z <$ ECR, $B_z \simeq$ ECR, and $B_z >$ ECR, as shown in Fig. 12(a)–(c), respectively. Measurements of injected power, reflected MW power, electrical-biased probe saturation current, and emitted plasma light were conducted, revealing a structure of two stages for breakdown process. We called the early breakdown stage as MW coupling, where the MW power matching is in progress under a low ionization rate, and fast coupling changes between MWs and the weak plasma inside the chamber are taking place. The second stage is the *plasma formation*, during which light emission increment is associated to an ionization rate increment and where saturation probe current is rapidly reached. During this last stage, the MW coupling is well established, and the absorbed energy density is good enough to produce plasma evolution to final steady-state parameters. Fig. 5 shows the structure that we proposed. According to such interpretation, this paper has been conducted on the basis of measurements of MW coupling and plasma formation times for the three magnetic field configurations, two different hydrogen operation pressures, and scanning of power values and duty cycles to establish typical breakdown times. Tables II–IV show a brief data summary with maximum and minimum measured times to keep in mind the range of values recorded. Note that breakdown times are not necessarily the sum of previous values in such tables because maximum and minimum values normally are not coincident in surfaces, as shown in Figs. 7–12.

For $B_z <$ ECR and a relative low hydrogen pressure of 3.8×10^{-3}mbar, breakdown is dominated by instabilities that determine a narrow operation range where measurements can be done. Low light emission and also low probe electrical

TABLE II
SUMMARY OF BREAKDOWN MEASUREMENTS FOR $B_z <$ ECR: PROFILE (a) AT FIG. 2

	3.8 x $10^{-3}mb$		6.2 x $10^{-3}mb$		*Remarks*
Times	Min.	Max.	Min.	Max.	
MW Coupling	40	105	20	50	Unstable behavior.
Plasma Formation	40	80	60	150	Narrow parameter operation range.
Breakdown	60	170	60	190	Low light emission.

TABLE III
SUMMARY OF BREAKDOWN MEASUREMENTS FOR $B_z \simeq$ ECR: SEE PROFILE (b) AT FIG. 2

	3.8 x $10^{-3}mb$		6.2 x $10^{-3}mb$		*Remarks*
Times	Min.	Max.	Min.	Max.	
MW Coupling	40	55	10	30	Good coupling and high light emission.
Plasma Formation	40	90	40	130	Unstable area for high duty
Breakdown	60	150	60	150	cycles an low powers.

TABLE IV
SUMMARY OF BREAKDOWN MEASUREMENTS FOR $B_z >$ ECR: SEE PROFILE (c) AT FIG. 2

	3.8 x $10^{-3}mb$		6.2 x $10^{-3}mb$		*Remarks*
Times	Min.	Max.	Min.	Max.	
MW Coupling	20	120	10	35	Stable behavior with high light emission
Plasma Formation	20	90	30	85	Unstable area for high duty
Breakdown	50	170	50	110	cycles an low powers.

current are symptoms of low density and temperature plasma. However, if the pressure is increased to 6.2×10^{-3}mbar, then the behavior is significantly improved, showing just a small working area of power values and duty cycles where instabilities and jitter are determinant at low power values and high duty cycles.

For $B_z \simeq$ ECR, the general behavior is characterized by a good MW coupling and emission light in a wide range of power values and duty cycles for the two hydrogen pressures under study. While MW coupling times show small variations, plasma times reach an instability area for low power values and high duty cycles that affects the total breakdown time behavior.

For $B_z >$ ECR and a relative low hydrogen pressure of 3.8×10^{-3}mbar, breakdown shows strong dependence of injected MW power where best coupling times are obtained for low duty cycles and high MW power values. This effect is moderated significantly when a higher hydrogen pressure of 6.2×10^{-3}mbar is used.

In general, the process with deeper impact over total breakdown is MW coupling, which dominates the general behavior. Disregarding the case $B_z <$ ECR where range operation is too small, coupling times present a smooth behavior with a relative small variation. The measurements P_i and P_r suggest a process associated to the drop of the electric field strength inside the plasma chamber [9]–[11]. At the beginning, the power absorption is poor, allowing the electric field strength in the plasma chamber to reach characteristic values for the coupling system and cavity, but once the ionization process starts, the absorption became important and the electric field drops. In all cases, an increment in breakdown time for high duty cycles and low power values is reported, whereas the best situations for good MW couplings are observed for high MW power values and low duty cycles. On the other hand, it is remarkable that the measurements of injected and reflected power are not enough to describe the full breakdown process because it is not sensible to changes associated to plasma formation stage. This fact should be considered for developers of automatic plasma optimization control systems based on measurements of injected and reflected power only.

A simple model based on the influence of seed electrons remaining in the neutral gas between pulses is developed with the goal to describe our experimental data as a function of duty cycle and power. The diffusive nature of the dynamics of seed electrons dynamic during the switch-off time between pulses is demonstrated in coincidence with experimental data of other experiments [17]. Calculations show good agreement with our experimental data for the case in which ECR magnetic field profile has been used but also show a mismatch for the magnetic field profile over ECR. A further research on this point is the aim of our near future work.

ACKNOWLEDGMENT

The authors would like to thank F. J. Bermejo for his continuous support, O. Tarvainen for his useful discussions, and R. Martinez for his help during reactor commissioning.

REFERENCES

[1] J. Lettry, M. Kronberger, R. Scrivens, E. Chaudet, D. Faircloth, G. Favre, J. M. Geisser, D. Küchler, S. Mathot, O. Midttun, M. Paoluzzi, C. Schmitzer, and D. Steyaert, "Hight duty factor plasma generator for CERN's Superconducting Proton Linac," *Rev. Sci. Instrum.*, vol. 81, no. 2, pp. 02A723-1–02A723-3, Feb. 2010.

[2] D. Leitner, C. Lyneis, S. Abbott, D. Collins, R. Dwinell, M. Galloway, M. Leitner, and D. Todd, "Next generation ECR ion sources: First results of the superconducting 28 GHz ECRIS—VENUS," *Nucl. Instrum. Method Phys. Res. B*, vol. 235, no. 1–4, pp. 486–493, Jul. 2005.

[3] P. Sortais, J. L. Bouly, J. Curdy, T. Lamy, P. Sole, T. Thuillier, J. L. Vieux-Rochaz, and D. Voulot, "ECRIS development for stable and radioactive pulsed beams," *Rev. Sci. Instrum.*, vol. 75, no. 5, pp. 1610–1612, May 2004.

[4] H. Shidara, Y. Nakashima, T. Imai, T. Kariya, R. Minami, M. Ichimura, and M. Yoshikawa, "EC wave plasma breakdown on GAMMA 10 device," *Fusion Eng. Des.*, vol. 86, no. 6–8, pp. 913–915, Oct. 2011.
[5] S. K. Sharma, H. Zushi, I. Takagi, Y. Hisano, T. Shikama, S. Morita, T. Tanabe, N. Yoshida, M. Sakamoto, Y. Higashizono, K. Hanada, M. Hasegawa, K. Nakamura, H. Idei, K. N. Sato, S. Kawasaki, H. Nakashima, A. Higashijima, Y. Nakashima, Y. Hatano, A. Sagara, Y. Nakamura, N. Ashikawa, T. Maekawa, Y. Kishimoto, and Y. Takase, "Permeation measurements for investigation atomic hydrogen flux and wall pumping/fuelling in QUEST," *J. Nucl. Mater.*, vol. 420, no. 1–3, pp. 83–93, Jan. 2012.
[6] O. Tarvainen, T. Ropponen, V. Toivanen, J. Ärje, and H. Koivisto, "Plasma breakdown diagnostics with the biased disc of electron cyclotron resonance ion source," *Plasma Sources Sci. Technol.*, vol. 18, no. 3, p. 035018, Aug. 2009.
[7] H. Bäcker, J. W. Bradley, P. J. Kelly, and R. D. Arnell, "Using Langmuir probes to measure the plasma decay rates in pulsed RF magnetron discharges," *J. Phys. D, Appl. Phys.*, vol. 34, no. 18, pp. 2709–2714, Sep. 2001.
[8] T. Ropponen, O. Tarvainen, I. Izotov, J. Noland, V. Toivanen, G. Machicoane, D. Leitner, H. Koivisto, T. Kalvas, P. Peura, P. Jones, V. Skalyga, and V. Zorin, "Studies of plasma breakdown and electron heating on 14GHz ECR ion source through measurement of plasma bremsstrahlung," *Plasma Sources Sci. Technol.*, vol. 20, no. 5, p. 055007, Oct. 2011.
[9] C. Lyneis, J. Benitez, D. Leitner, J. Noland, M. Strohmeier, H. Kovisto, and O. Tarvainien, "Charaterization of the microwave coupling to the plasma chamber of the LBL ECR ion source," in *Proc. ECRIS*, Grenoble, France, 2010, pp. 162–164.
[10] L. Celona, S. Gammino, F. Maimone, D. Mascali, N. Gambino, R. Miracoli, and G. Ciavola, "Observations of resonant modes formation in microwave generated magnetized plasmas," *Eur. Phys. J. D*, vol. 61, no. 1, pp. 107–115, Jan. 2011.
[11] L. Celona, S. Gammino, G. Ciavola, F. Maimone, and D. Mascali, "Microwave to plasma coupling in electron cyclotron resonance and microwave ion sources (invited)," *Rev. Sci. Instrum.*, vol. 81, no. 2, pp. 02A333-1–02A333-6, Feb. 2010.
[12] T. Ropponen, O. Tarvainen, V. Toivanen, P. Peura, P. Jones, T. Kalvas, H. Koivisto, J. Noland, and D. Leitner, "The effect of RF pulse pattern on bremsstralung and ion current time evolution of an ECRIS," *Rev. Sci. Instrum.*, vol. 81, no. 2, pp. 02A302-1–02A302-3, Feb. 2010.
[13] S. Djekic, I. Bustinduy, D. Cortazar, D. Fernandez-Cañoto, H. Hassanzadegan, J. L. Munoz, D. de Cos, F. J. Bermejo, M. A. Carrera, J. H. Galipienzo, V. Etxebarria, J. Jugo, J. Portilla, J. Feuchtwanger, I. Rueda, and J. Lucas, "Preliminary design of BLISI, an off resonance microwave proton source," in *Proc. ECRIS*, Grenoble, France, 2010.
[14] H. R. Griem, *Principles of Plasma Spectroscopy*. New York: Cambridge Univ. Press, 1997, pp. 248–250, cap. 9.
[15] E. Gray and D. Kerr, "The diffusion equation with a quadratic loss term applied to electron volume recombination in a plasma," *Ann. Phys.*, vol. 17, no. 2, pp. 276–300, Feb. 1962.
[16] R. J. Goldston and P. H. Rutherford, *Introduction to Plasma Physics*. New York: Taylor & Francis, 1995, p. 152, cap. 10.
[17] O. Tarvainen, T. Ropponen, V. Toivanen, T. Kalvas, J. Ärje, and H. Koivisto, "Diagnostics of plasma decay and afterglow transient of an electron cyclotron resonance ion source," *Plasma Sources Sci. Technol.*, vol. 19, no. 4, pp. 045027-1–045027-13, Aug. 2010.
[18] G. Guest, *Electron Cyclotron Heating of Plasmas*. Weinheim, Germany: Wiley, 2009, pp. 103–114, cap. 6.

O. Daniel Cortázar was born in Rosario, Argentina, in 1960. He received the B.S. degree from National University of Central Buenos Aires, Tandil, Argentina, in 1986; the Ph.D. degree in plasma physics from National University of Mar del Plata, Buenos Aires, Argentina, in 1990; and the Postdoctoral degree in X-ray lasers from Colorado State University, Fort Collins, in 1994.

He is currently a Group Head with Power Electronics Group, European Spallation Source Bilbao, Leioa, Spain, and a Professor with the University of Castilla-La Mancha, Ciudad Real, Spain. His research interests include electron cyclotron resonance plasma sources, plasma diagnostics, lasers, and power electronics.

Ana Megía-Macías was born in Alcazar de San Juan, Spain, in 1985. She received the B.S. degree in industrial engineering from the University of Castilla-La Mancha, Ciudad Real, Spain, in 2008.

In 2009, she was a Research Assistant with the R&D Group, Sheffield Forgemaster Ltd., Sheffield, U.K. In 2010, she was a Engineering Development Chief with the Metal Institute of Tomelloso, Ciudad Real, in 2010. She is currently a Research Assistant with European Spallation Source Bilbao, Leioa, Spain. Her research interest include electron cyclotron resonance plasma sources and plasma diagnostics.

Alvaro Vizcaíno-de-Julián was born in Almagro, Spain, in 1985. He received the B.S. degree in industrial engineering from the University of Castilla-La Mancha, Ciudad Real, Spain, in 2008.

In 2009, he was a Research Assistant with the R&D Group, Sheffield Forgemaster Ltd., Sheffield, U.K. He was a Research Fellow with the Renewable Energy Research Center of Castilla-La Mancha, Albacete, Spain. He is currently a Research Assistant with European Spallation Source Bilbao, Leioa, Spain. His research interests include electron cyclotron resonance plasma sources, plasma diagnostics, and power electronics.